Proceedings of DETC'03
ASME 2003 Design Engineering Technical Conferences and Computers and Information in Engineering Conference
Chicago, Illinois USA, September 2-6, 2003

DETC2003/PTG-48055

DYNAMIC ANALYSIS OF SLIDING FRICTION IN A GEAR PAIR

Rajendra Gunda
Acoustics and Dynamics Laboratory
The Ohio State University
Columbus, OH 43210-1107
Email: gunda.2@osu.edu

Rajendra Singh*
Acoustics and Dynamics Laboratory
The Ohio State University
Columbus, OH 43210-1107
Email: singh.3@osu.edu

ABSTRACT

Chief objective of this article is to evaluate the role of sliding friction in gear dynamics, and more specifically the effect of the periodic variations in mesh stiffness, load distribution and friction torque during a mesh cycle. A non-unity speed ratio spur gear is considered. Only the torsional degree of freedom of the gear pair, with ideal Coulomb friction law, is analyzed. Previous studies by Vaishya and Singh [1–3] make idealized assumptions about temporal (or spatial) variation of mesh stiffness and load sharing in order to obtain more tractable analytical solutions. In our formulation, an accurate Finite Element/Contact Mechanics analysis code [4] is run in the static mode to compute the mesh stiffness and load distribution at every time instant of the mesh. The computed parametric variation of stiffness is then incorporated into our dynamic formulation that includes frictional torques. Next, we use appropriate numerical techniques to solve for the dynamic response in time domain. This study, though preliminary in nature, examines the effects of pinion speed, coefficient of friction and mean input torque. This, along with work in progress, should yield further insights into the role of friction sources in gear vibro-acoustics.

NOMENCLATURE

T_p, T_g Mean input pinion torque and gear braking torque
ϕ Pressure angle
r_{bp}, r_{bg} Base radius of pinion, gear
Ω_p, Ω_g Angular speed of pinion, gear
t_b Time instant when pair # 0 is at LPSTC (point B)
t_p Time instant when pair # 0 is at pitch point P
t_c Time period of one mesh cycle
λ Base pitch
θ_p, θ_g Vibratory motion of pinion, gear
$k_o(t), k_1(t)$ Stiffness of pair # 0 and pair # 1
$c_o(t), c_1(t)$ Damping of pair # 0 and pair # 1
$N_0(t), N_1(t)$ Normal tooth loads in pair # 0 and pair # 1
$F_0(t), F_1(t)$ Frictional forces in pair # 0 and pair # 1
μ Coefficient of Coulomb friction
$x_{1p}(t), x_{0p}(t)$ Moment arms for pinion friction torques
$x_{1g}(t), x_{0g}(t)$ Moment arms for gear friction torques
J_p, J_g Polar moment of inertia of pinion, gear
$J_e/J_b = J_p \cdot J_g/(J_g \cdot r_{bp}^2 + J_p \cdot r_{bg}^2)$ Effective polar moment of inertia of the SDOF system
$\varepsilon(t)$ Static transmission error (STE)
$\varepsilon_p(t)$ Profile error component of STE
$\varepsilon_l(t)$ Elastic deformation component of STE
$\delta(t)$ Dynamic transmission error (DTE)

INTRODUCTION

This article extends the recent analytical investigations by Vaishya and Singh [1–3]. They employed simplistic, yet ideal, periodic variations of load distributions, mesh stiffness, coefficient of friction and friction torque based on the assumption that load is shared equally among all the teeth in contact. In this paper, we relax this assumption and calculate the realistic stiffness variations as a function of normalized time, and then predict the

*Corresponding Author.

dynamic transmission error (DTE) of a spur gear pair using a single degree of freedom torsional model. Resulting time histories and frequency spectra are compared with those reported earlier by Vaishya and Singh [1–3].

The literature on sliding friction is sparse [1–3, 5–9], although it is believed to be one of the primary excitations for noise and vibration in geared systems. For a detailed review of the relevant publications, refer to Vaishya and Singh [1–3] as well as the experimental and computational studies by Houser et. al. [5, 6], Iida et. al. [7], and Velex and Cahouet [8].

PROBLEM FORMULATION

The schematic in Figure 1 illustrates the counter shaft non-unity contact ratio spur gear pair considered for analysis. Refer to Table 1 for geometrical design parameters of our example case. The pinion and gear are modeled as rigid disks, each with one rotational degree of freedom.

Figure 1 is a snapshot of the system at the beginning of the mesh cycle, $(t = 0)$. At this time instant, the pair # 0 (teeth shown in green) just comes into mesh at point A. Pair # 1 (teeth shown in red) is in contact at point C along the line of contact. Point C is the highest point of single tooth contact (HPSTC). As the gears roll, when pair # 0 approaches point B (LPSTC) at $t = t_b$, pair # 1 leaves contact. At $t = t_p$, pair # 0 passes through the pitch point P. The relative sliding velocity of the pinion with respect to the gear is reversed at $t = t_p$ resulting in reversal of friction force. This provides an impulsive excitation to the system. Pair # 1 goes through point C at $t = t_c$, completing one mesh cycle (t_c). Timing of these critical events in a mesh cycle is determined from the undeformed gear geometry. The length AC is equal to one base pitch, λ. The mesh cycle time is given as $t_c = \frac{\lambda}{\Omega_p r_{bp}}$, $\frac{t_b}{t_c} = \frac{AB}{\lambda}$ and $\frac{t_p}{t_c} = \frac{AP}{\lambda}$.

An input torque T_p is applied to the pinion rotating at a nominal angular velocity Ω_p. The mean braking torque T_g on the gear and its angular velocity Ω_g obey basic gear kinematics. Superposed on this kinematic motion is an oscillatory component. Here θ_p and θ_g denote these vibratory motions for the pinion and the gear respectively.

The mesh stiffness of pair # 0 and pair # 1 are denoted by $k_0(t)$, and $k_1(t)$ respectively and are obtained by performing static analysis using External2D software [4], which is based on an accurate Contact Mechanics/Finite Element (CM/FE) formulation. At each roll position, the gear rotation is constrained and a known torque is applied to the pinion. The tooth contact forces $N_0(t)$, $N_1(t)$ and pinion deflection θ_p are computed by External2D using a quadratic programming approach. Reference [10] contains details of the CM/FE formulation.

The mesh stiffness $k_0(t)$, and $k_1(t)$ are then given as $k_0(t) = \frac{N_0(t)}{r_{bp}\theta_p(t)}$ and $k_1(t) = \frac{N_1(t)}{r_{bp}\theta_p(t)}$. Here $\varepsilon_l(t) = r_{bp}\theta_p(t)$ is the loaded static transmission error for gears with perfect involute teeth under static loaded condition. Since we have a periodic system, the mesh stiffness functions $k_0(t)$, and $k_1(t)$ can also be obtained by following the tooth pair # 0 *for two complete meshing cycles*. If the stiffness function for pair # 0 over two mesh cycles is represented by $k(t)$, then following equation represent stiffness functions $k_0(t)$ and $k_1(t)$ in a mesh cycle, which are valid for *any* value of time t.

$$\begin{aligned} k_0(t) &= k(t_c + \mathrm{mod}\,(t, t_c)) \\ k_1(t) &= k(\mathrm{mod}\,(t, t_c)) \end{aligned} \tag{1}$$

In Equation 1, mod is the modulus function, which is signed remainder after division,

$$\mathrm{mod}\,(x, y) = x - y \cdot \mathrm{floor}(x/y) \quad \text{if} \quad y \neq 0 \tag{2}$$

where x and y are real numbers and floor(x) is the nearest integer less than x.

Since the Coulomb friction law is considered for this analysis, the friction force magnitude (F_f) is proportional to the normal tooth load (N) as $F_f = \mu N$ and relative sliding velocity between the bodies at the point of contact governs its direction. The coefficient of friction μ is taken to be constant, and not function of relative sliding velocity. Sliding velocity is computed based on nominal kinematic motion, resulting in a linear time varying system of governing equations as opposed to a NLTV system [1–3].

Figure 2 shows the applied and internal reaction forces acting on the pinion (For the sake of clarity the forces on the gear are not shown. They are equal in magnitude but opposite in direction to the pinion forces). The frictional force $F_0(t)$ in pair # 0 is in opposite direction to pair # 1. The direction of friction force $F_0(t)$ will reverse as pair # 0 goes through the pitch point P. Here XC_1 and XC_0 are the moment arms for the friction forces $F_1(t)$ and $F_0(t)$.They are given as

$$\begin{aligned} \mathrm{XC}_1 &= x_{1p}(t) = \mathrm{XA} + \mathrm{mod}\,(\Omega_p r_{bp} t, \lambda) \\ \mathrm{XC}_0 &= x_{0p}(t) = \mathrm{XC} + \mathrm{mod}\,(\Omega_p r_{bp} t, \lambda) \end{aligned} \tag{3}$$

Similarly, the corresponding moment arms for the friction forces on the gear are given as

$$\begin{aligned} \mathrm{YC}_1 &= x_{1g}(t) = \mathrm{YA} - \mathrm{mod}\,(\Omega_p r_{bp} t, \lambda) \\ \mathrm{YC}_0 &= x_{0g}(t) = \mathrm{YC} - \mathrm{mod}\,(\Omega_p r_{bp} t, \lambda) \end{aligned} \tag{4}$$

The equations of motion for pinion and gear are as follows.

$$T_p - (N_1(t)+N_0(t))\cdot r_{bp} + F_1(t)\cdot \mathrm{sgn}(AP - \mathrm{mod}(\Omega_p r_{bp} t, \lambda))\cdot x_{1p}(t) - F_0(t)\cdot x_{0p}(t) = J_p \ddot{\theta}_p(t) \quad (5)$$

$$T_g + (N_1(t)+N_0(t))\cdot r_{bg} - F_1(t)\cdot \mathrm{sgn}(AP - \mathrm{mod}(\Omega_p r_{bp} t, \lambda))\cdot x_{1g}(t) + F_0(t)\cdot x_{0g}(t) = J_g \ddot{\theta}_g(t) \quad (6)$$

In Equations 5 and 6, sgn is the signum function defined as

$$\begin{aligned} \mathrm{sgn}(x) &= 1, \text{if } x > 0 \\ &= 0, \text{if } x = 0 \\ &= -1, \text{if } x < 0 \end{aligned} \quad (7)$$

The dynamic transmission error is defined as $\delta(t) = r_{bp}\theta_p(t) - r_{bg}\theta_g(t)$. The normal loads $N_i(t)$ are given as

$$N_i(t) = k_i(t)\cdot(\delta(t) - \varepsilon_p(t)) + c_i(t)\cdot(\dot{\delta}(t) - \dot{\varepsilon}_p) \quad (8)$$

where $\varepsilon_p(t)$ is the profile error component of the static transmission error. The deformation component of static transmission error is not included in Equation 8, since it is already accounted for in terms of the mesh stiffness . After algebraic manipulation of Equations 5 and 6, to eliminate $\theta_p(t)$ and $\theta_g(t)$ in terms of DTE $\delta(t)$, the governing equation for DTE $\delta(t)$ is obtained as

$$\begin{aligned} &\tfrac{J_e}{J_b}\ddot{\delta}(t) + (c_1(t)+c_0(t))\dot{\delta}(t) + (k_1(t)+k_0(t))\cdot\delta(t) \\ &-\mu k_1(t)\delta(t)\tfrac{\left(x_{1p}(t)J_g r_{bp} + x_{1g}(t)J_p r_{bg}\right)}{J_b}\cdot \mathrm{sgn}(AP - \mathrm{mod}(\Omega_p r_{bp} t, \lambda)) \\ &+\mu k_0(t)\delta(t)\tfrac{\left(x_{0p}(t)J_g r_{bp} + x_{0g}(t)J_p r_{bg}\right)}{J_b} = \\ &\tfrac{T_e}{J_b} + (k_1(t)+k_0(t))\cdot\varepsilon_p(t) + (c_1(t)+c_0(t))\dot{\varepsilon}_p(t) \\ &-\mu k_1(t)\varepsilon_p(t)\tfrac{\left(x_{1p}(t)J_g r_{bp} + x_{1g}(t)J_p r_{bg}\right)}{J_b}\cdot \mathrm{sgn}(AP - \mathrm{mod}(\Omega_p r_{bp} t, \lambda)) \\ &+\mu k_0(t)\varepsilon_p(t)\tfrac{\left(x_{0p}(t)J_g r_{bp} + x_{0g}(t)J_p r_{bg}\right)}{J_b} \end{aligned} \quad (9)$$

Equation 9 is recast in state-space form and solved by numerical time integration as shown in Equation 10.

$$\frac{d}{dt}\begin{pmatrix} y_1 \\ y_2 \end{pmatrix} = \begin{pmatrix} y_2 \\ g(y_1, y_2, t) \end{pmatrix} \text{ where } y_1 = \delta \text{ and } y_2 = \dot{\delta} \quad (10)$$

In Equation 10, $g(y_1, y_2, t)$ is a function obtained from Equation 9.

COMPARISON OF STIFFNESS MODELS

The gear design parameters for NASA-ART gear set studied in our analysis are given in Table 1. Following the procedure described in the problem formulation section, the stiffness functions $k_0(t)$ and $k_1(t)$ are computed from the tooth loads and the static loaded transmission error $\varepsilon_l(t)$ (shown in Figure 3). The stiffness functions $k_0(t)$, $k_1(t)$ and the combined stiffness $k(t)$ are shown in Figure 4. From Figure 4, it is also clear that stiffness functions $k_0(t)$, $k_1(t)$, can also be obtained by following the pair # 0 for two mesh cycles. $k_0(t)$ and $k_1(t)$ are just different portions of the curve $k(t)$ as described by Equation 1. It is also seen the load on the pair coming into mesh, namely pair # 0 gradually increases starting from zero load.

Existing models by Vaishya and Singh [1–3] make use of the equal load sharing assumption, resulting in sudden changes in tooth loads as they enter or leave contact. In the current formulation, the only source of impulsive excitation occurs at the pitch point due to the friction force reversal. In Figure 5, the variation of total mesh stiffness from both formulations is presented. Formulations [1–3] lead to piecewise constant, but discontinuous total stiffness function (square wave in Figure 5), while our approach leads to stiffness function that is continuous in time.

RESULTS AND DISCUSSION

In the current study, the component of static transmission error due to profile deviations is not considered as the gear teeth are taken as perfect involutes. Hence the only non-zero term in Equation 9 exciting the system is the applied mean torque. Several combinations of the coefficient of friction μ, damping ratio ξ, input torque T_p, and pinion speed Ω_p are considered in our simulations to study the influence of key system parameters on DTE $\delta(t)$.

Effect of Friction at Low Speed

Figure 6 shows the physical significance of introducing frictional forces in the model. Since Ω_p (2.4 rpm) is very small, the dynamic effects are insignificant. Hence the DTE for case without friction is identical to the $\varepsilon_l(t)$ curve in Figure 3. However, friction changes the shape of the DTE curve. In the time interval $t \in [0, t_p)$, the friction torque on the pinion opposes the torque due to the normal load (Figure 2), resulting in a higher value of normal load to maintain static equilibrium. Friction increases the peak-peak value δ of compared to $\varepsilon_l(t)$. For the remainder of the mesh cycle $t \in [t_p, t_c)$, friction torque acts in the same direction as normal load torque. Thus a smaller value of normal load is sufficient to maintain static equilibrium. These effects are clearly seen from Figure 6.

Table 1. GEAR GEOMETRY AND DESIGN PARAMETERS FOR NASA-ART GEAR SET.

	Pinion	**Gear**
Number of Teeth	25	31
Diametral Pitch, in^{-1}	8	8
Pressure Angle, deg	25	25
Outside Diameter, in	3.372	4.117
Root Diameter, in	2.811	3.561
Face width, in	1.250	1.250
Tooth Thickness, in	0.196	0.196
Nominal Pitch Diameter, in	3.125	3.875
Rim Diameter, in	2.250	3.005
Addendum Radius, in	1.686	2.058
Mass, $\text{lbf} \cdot \text{sec}^2 \cdot \text{in}^{-1}$	6.72E-03	1.04E-02
Polar Moment of Inertia, $\text{lbf} \cdot \text{sec}^2 \cdot \text{in}$	8.48E-03	2.00E-02
Center Distance,in	3.500	
Profile Contact Ratio	1.43	
Elastic Modulus, psi	30 E6	
Density, $\text{lbf} \cdot \text{sec}^{-2} \cdot \text{in}^{-4}$	7.30E-04	
Poisson's Ratio	0.3	
Input Torque, $\text{lbf} \cdot \text{in}$	2000	

STIFFNESS MODEL COMPARISON

Results comparing piecewise constant stiffness model to our stiffness model show that in our model, due to the smooth variation of tooth loads for gear tooth entering and leaving the mesh, DTE has a transient excitation and response only when the contact passes through the pitch point. Formulations [1–3] exhibit transient response at the beginning of mesh cycle, LPSTC and on crossing the pitch point. This phenomenon is illustrated in Figure 7.

EFFECT OF FRICTION AT HIGHER SPEEDS

The results of numerical simulations for a range of pinion speeds from 1000 rpm to 15000 rpm are plotted in Figures 8–13, as waterfall plots, order and difference colormaps. For each of the speeds considered, the DTE $\delta(t)$ was computed with and without including the frictional effects.

In Figures 8 and 9, the computed DTE has contributions both from variable elasticity and frictional effects. The first ten harmonics of the meshing frequency are clearly seen. For the NASA-ART gears considered, assuming an average mesh stiffness of 4.56e6 lbf/in, the system has a torsional mode at 6716 Hz, which coincides with the first tooth meshing frequency at 16118 rpm. Figures 8 and 9 clearly show amplification in the system response when any harmonic of the gear meshing frequency crosses over the natural frequency ω_n.

Figures 10, 11 are DTE computation results when $\mu = 0$. In Figures 12 and 13, the quantity plotted is $\log\left(\frac{\delta_\mu}{\delta}\right)$. This measure is meant to isolate the friction effect only, since the remaining parameters are unchanged between the two simulations. From Figures 12 and 13 it is very clear that the *second harmonic of the tooth mesh frequency is increased due to friction.*

EFFECT OF MEAN TORQUE

In Figure 14, the variation of peak-to-peak value of DTE $\delta(t)$, with input torque T_p is plotted at a pinion speed Ω_p of 2000 rpm. From Figure 14, it is clear that peak-to-peak value of DTE $\delta(t)$ increases with an increase in input torque T_p. Also, for a given value of input torque T_p, friction has an effect of increasing the DTE.

CONCLUSION

In this paper, an accurate stiffness model is used to represent the variation of tooth mesh stiffness and load sharing between pairs in mesh. The governing equations are then numerically integrated to compute the dynamic transmission error Existing formulations [1-3] yield transient response when a pair enters or leaves the mesh. In contrast, our formulation yields transient response only due to the reversal of friction force at the pitch point. Since the lumped parameter model is computationally efficient, it can be used to quickly study the effect of large number of system parameters. Finally, one of the main effects of friction that has been observed thus far is the increase in magnitude of the second harmonic of the tooth mesh frequency.

The work reported in this paper is preliminary in nature as we have have embarked upon a comprehensive project that will examine both linear time-varying and nonlinear effects of sliding friction in spur and helical gears. Concurrently, we will comparatively evaluate analytical (lumped parameter models) and computational [9] approaches. Future work will also focus on experimental studies, based on the observations reported here, as well as work in progress.

ACKNOWLEDGMENT

This material is based upon work supported by the U. S. Army Research Laboratory and the U. S. Army Research Of-

fice under grant number DAAD19-02-1-0334 (Project Monitor Dr. G. L. Anderson). The authors thank Dr. S. Vijayakar (Advanced Numerical Solutions, Inc.) for making available a copy of External2D gear analysis software, and for several interesting discussions. We also acknowledge discussions with Dr. D. R. Houser, as well as his support for experimental studies that are being planned.

REFERENCES

[1] Vaishya, M., and Singh, R., 2001. "Sliding friction induced non-linearity and parametric effects in gear dynamics". Journal of Sound and Vibration, **248** (4), pp. 671–694.

[2] Vaishya, M., and Singh, R., 2001. "Analysis of periodically varying gear mesh systems with coulomb friction using floquet theory". Journal of Sound and Vibration, **243** (3), pp. 525–545.

[3] Vaishya, M., and Singh, R., 2003. "Strategies for modeling friction in gear dynamics". *ASME Journal of Mechanical Design*. (In Print)

[4] ADVANCED NUMERICAL SOLUTIONS, INC., 2003. *External2D Users Manual*. Hilliard, OH.

[5] Hochmann, D., and Houser, D. R., 2000. "Friction forces as dynamic excitation source in involute spur and helical gearing". *Proceedings of DETC2000*, pp. 581–590.

[6] Borner, J., and Houser, D. R., 1996. "Friction and bending moments as gear noise excitations". SAE Transactions (961816).

[7] Iida, H., Tamura, A., and Yamada, Y., 1985. "Vibrational characteristics of friction between gear teeth". Bulletin of JSME, **28** (241), pp. 1512–1519.

[8] Velex, P., and Cahouet, V., 2000. "Experimental and numerical investigations on the influence of tooth friction in spur and helical gear dynamics". Proceedings of DETC2000 (PTG-14430), pp. 591–600.

[9] Ozguven, H. N., and Houser, D. R., 1988. "Dynamic analysis of high speed gears by using loaded static transmission error". Journal of Sound and Vibration, **125** (1), pp. 71–83.

[10] Parker, R. G., Vijayakar, S. M., and Imajo, T., 2000. "Nonlinear dynamic response of a spur gear pair: modeling and experimental comparisons". Journal of Sound and Vibration, **237** (3), pp. 435–455.

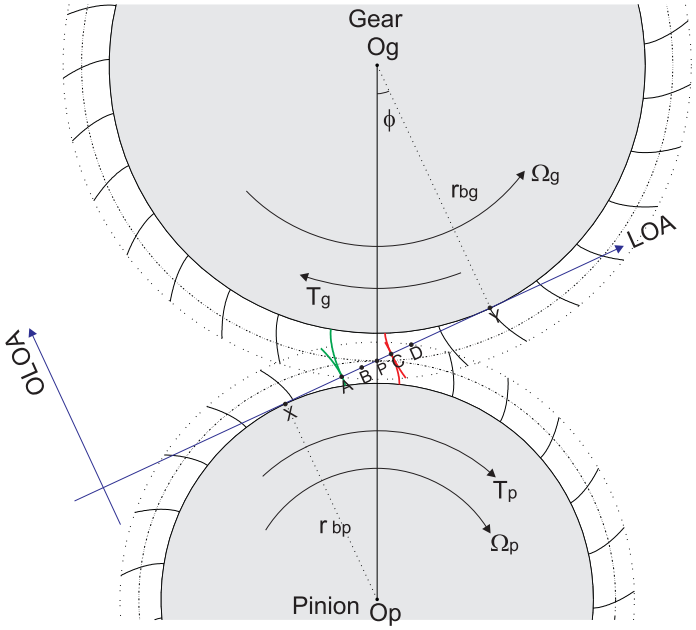

Figure 1. GEAR SYSTEM AND NOTATION.

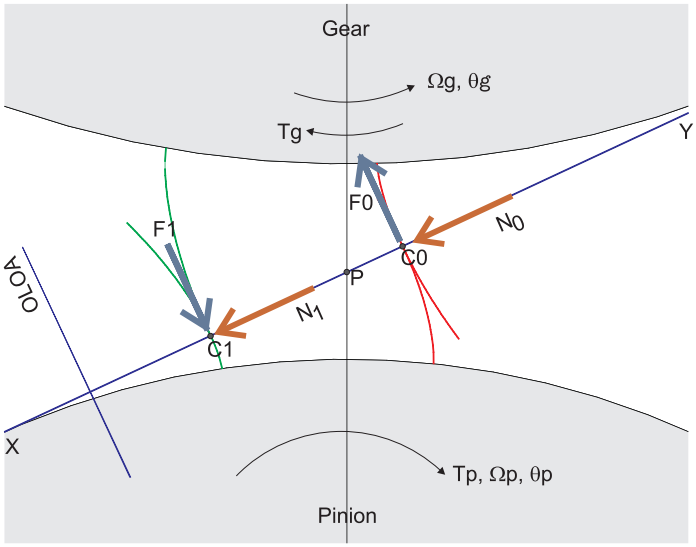

Figure 2. FREE BODY DIAGRAM FOR THE PINION.

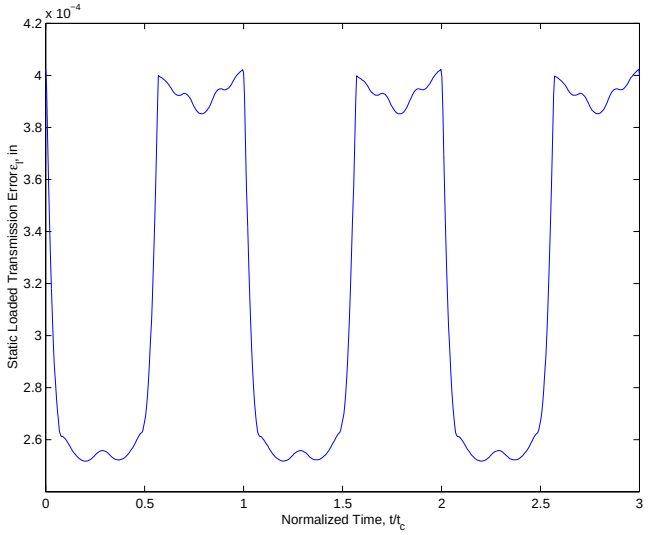

Figure 3. STATIC TRANSMISSION ERROR PREDICTION FROM EXTERNAL2D.

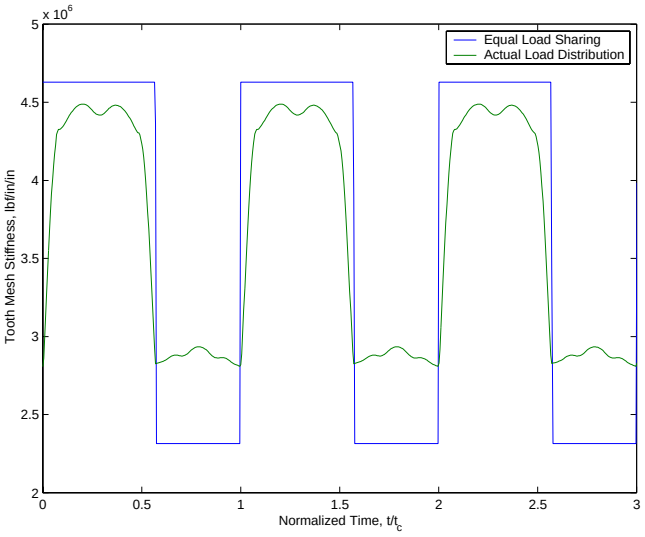

Figure 5. COMPARISION OF THE TWO STIFFNESS MODELS. KEY: BLUE LINE – EQUAL LOAD SHARING ASSUMPTION [1-3], GREEN LINE – ACTUAL LOAD SHARING.

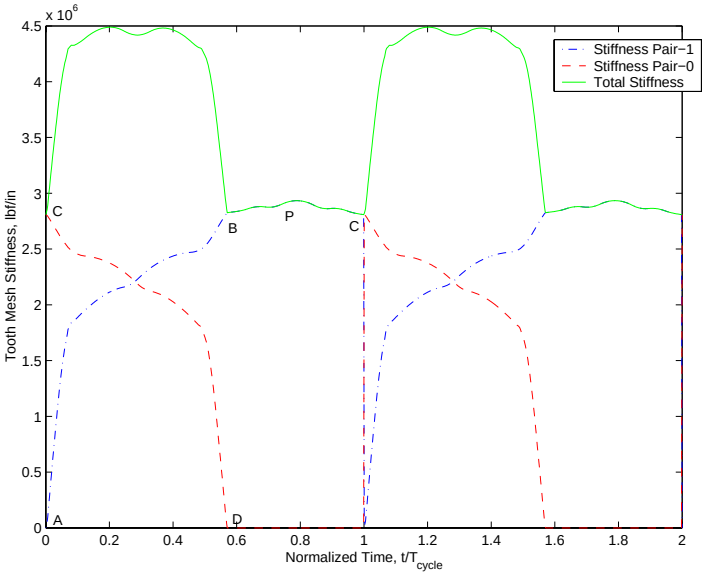

Figure 4. STIFFNESS FUNCTIONS. KEY: $k_0(t)$ – (RED LINE), $k_1(t)$ – (BLUE LINE), AND COMBINED STIFFNESS $k_1(t)$ – (GREEN LINE)

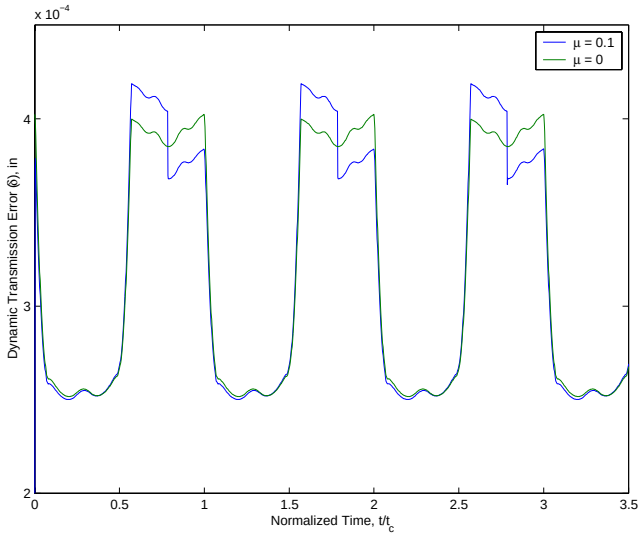

Figure 6. EFFECT OF FRICTION COEFFCIENT ON DTE. T_p = 2000 LBF-IN, $\Omega_p = 2.4$ RPM. KEY: BLUE LINE – $\mu = 0.1$, GREEN LINE – $\mu = 0$.

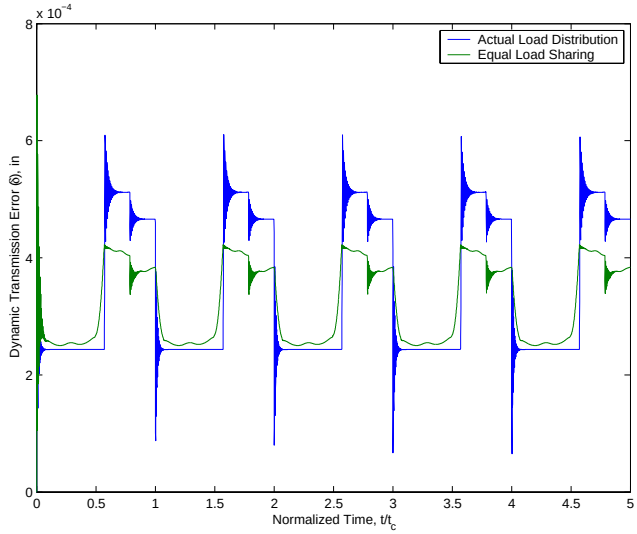

Figure 7. EFFECT OF STIFFNESS MODEL ON DTE. T_p = 2000 LBF-IN, $\Omega_p = 100$ RPM, $\mu = 0.1$. KEY: BLUE LINE – EQUAL LOAD SHARING ASSUMPTION [1-3], GREEN LINE – ACTUAL LOAD SHARING.

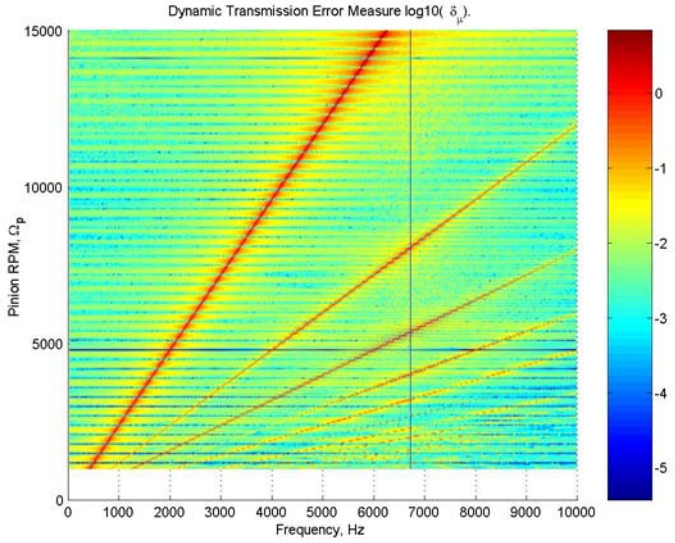

Figure 9. FREQUENCY VS. RPM VS. log10(δ_μ). T_p = 2000 LBF-IN, $\mu = 0.1$.

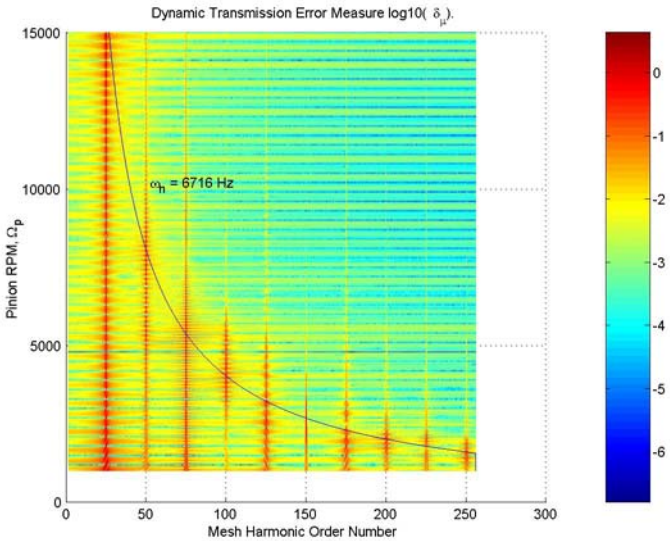

Figure 8. ORDER VS. RPM VS. log10(δ_μ). T_p = 2000 LBF-IN, $\mu = 0.1$.

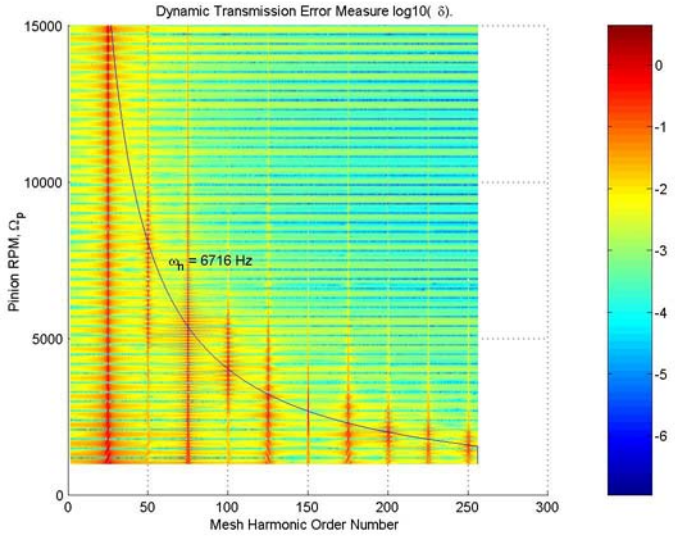

Figure 10. ORDER VS. RPM VS. log10(δ). T_p = 2000 LBF-IN, $\mu = 0$.

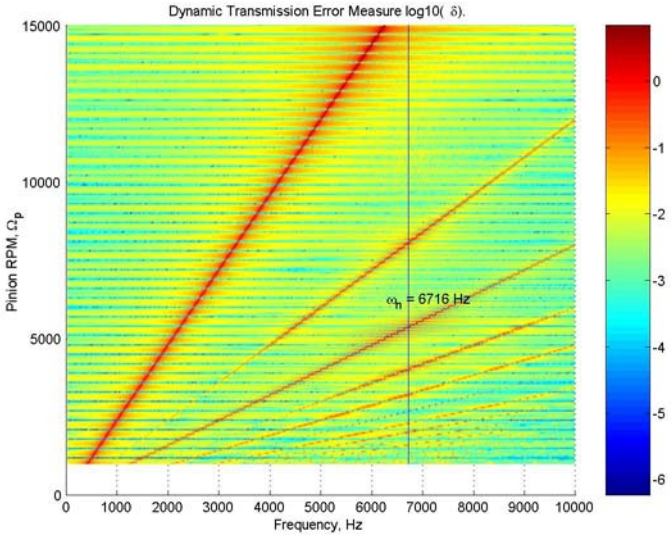

Figure 11. FREQUENCY VS. RPM VS. log10(δ). T_p = 2000 LBF-IN, $\mu = 0$.

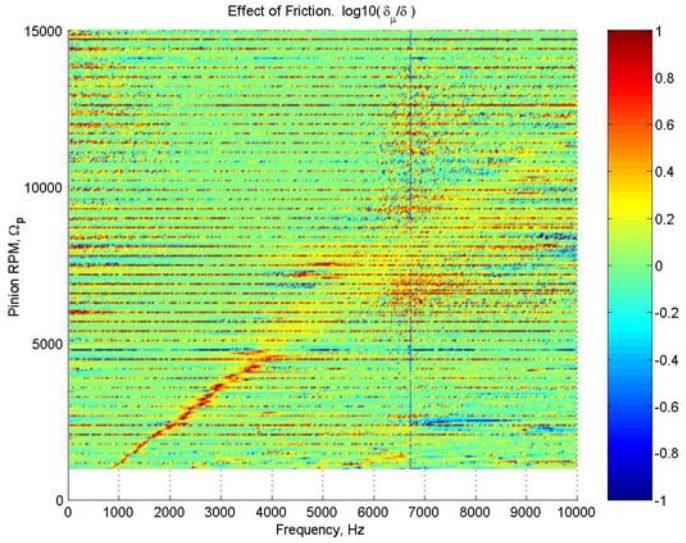

Figure 13. DIFFERENCE COLORMAP. FREQUENCY VS. PINION RPM VS $\log\left(\frac{\delta_\mu}{\delta}\right)$. T_p = 2000 LBF-IN.

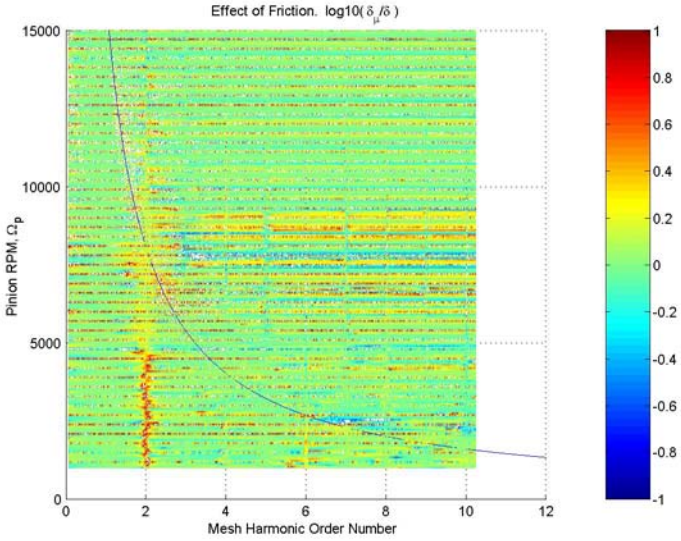

Figure 12. DIFFERENCE COLORMAP. ORDER VS. PINION RPM VS $\log\left(\frac{\delta_\mu}{\delta}\right)$. T_p = 2000 LBF-IN.

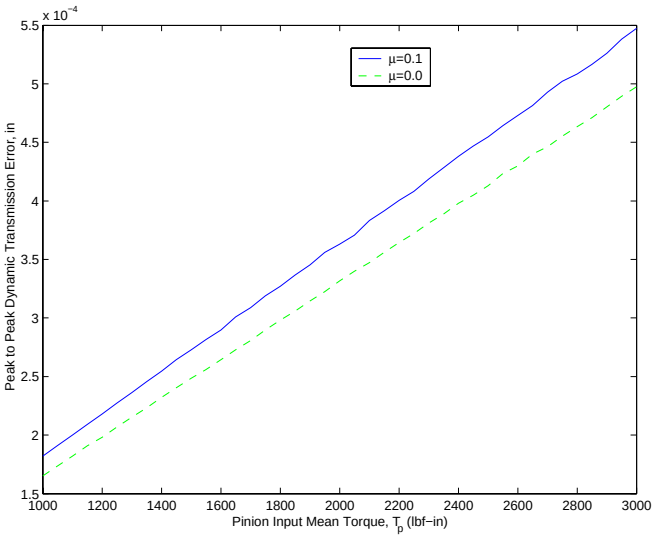

Figure 14. VARIATION OF PEAK TO PEAK VALUE OF DTE δ WITH INPUT TORQUE T_p. KEY: BLUE SOLID LINE – $\mu = 0.1$, GREEN DASHED LINE – $\mu = 0$. PINION ROTATIONAL SPEED $\Omega_p = 2000$ RPM.